Journal of Alloys and Compounds 488 (2009) 606–611

Contents lists available at ScienceDirect

Journal of Alloys and Compounds

journal homepage: www.elsevier.com/locate/jallcom

Optical properties of Nd^{3+} and Er^{3+} ions in fluoro-phosphate glasses: Effects of P_2O_5 concentration and laser applications

A. Flórez*, E.M. Ulloa, R. Cabanzo

Universidad Industrial de Santander, Escuela de Física, Laboratorio de Materiales Fotónicos, A. A. 678, Bucaramanga, Colombia

ARTICLE INFO

Article history:
Received 1 June 2008
Received in revised form 2 September 2009
Accepted 10 September 2009
Available online 18 November 2009

Keywords:
Inorganic, amorphous and optical materials
Solid state reaction
Optical properties

ABSTRACT

Materials based on fluoride glasses have been recognized as potential hosts for trivalent rare earth ions for different applications, such as fiber lasers. A broad range of stability, an appropriate refractive index and the optimization of the optical and mechanical properties are important characteristics that need to be improved in these new materials. In this work, we made a systematic study of the effect of substituting BaF_2 for P_2O_5 in the matrix: $35InF_3$–$20ZnF_2$–$(16-x)BaF_2$–xP_2O_5–$20SrF_2$–$6GaF_3$–$2NaF$–$1.0REF_3$, where RE = Nd^{3+}, Er^{3+}, with x = 4.0; 8.0; 12.0 and 16.0 molar concentration. In order to evaluate the material's thermal evolution, we obtained differential scanning calorimeter (DSC) measurements, noting the variations in the stability range. Measurements of the refractive index, absorption and luminescence at room temperature in the spectral range from 300 to 3200 nm were also obtained. An increase in refractive index with increasing P_2O_5 concentrations was observed. The behavior of phonons in the samples was observed through of the absorption intensity and the narrowing of the bands in the visible part of the spectrum; the width of the bands in the infrared region did not change. From the areas of the absorption bands, we calculated the oscillator strengths for the all of the samples, and using the Judd–Ofelt intensity model, we calculated the characteristic spectroscopic parameters. Furthermore, we analyzed the intensity parameter in Nd^{3+} and Er^{3+} doped glasses to determine the material's suitability for laser applications.

Published by Elsevier B.V.

1. Introduction

There have been numerous studies on fluoride glasses as host materials for trivalent rare earth ions in order to find potential applications in telecommunications, lasers, sensors, amplifiers, wave guides, and other photonic devices [1–5]. The wide range of transparency (up to ~10 μm) and low phonon energy make these materials important for new technologies [6].

Due to the prevalence of fluorine, these materials have a strong ionic character; thus, the weak ionic bonding in these materials and the heavy metallic ions explain the low resonance frequency characteristic of these glasses. As a result of the low resonance frequencies, these materials have low non-radiative losses that increase up-conversion efficiencies [7]. These characteristics make these materials good candidates for applications in laser technology [8]. At the moment, for the use of glasses in laser applications, phosphates have the best properties [9]. Fluoride glasses also have potential for applications in lasers, but further research is necessary to optimize their properties.

Of all lanthanide rare earths ions, Nd^{3+} has been extensively studied for lasers; therefore, almost all solid state lasers use Nd^{3+} as the active ion at present [10–12]. Except for Pm and Gd, all of the lanthanide ions has transitions that are useful for laser devices. Aside from Nd^{3+}, the Er^{3+} ion presents the best optical properties for photonic applications. However; aside from the well known problems related to the Ω_2 intensity parameter of Pr^{3+}, when transitions are described by the Judd–Ofelt theory [13–15], Pr^{3+} presents attractive properties such as low phonon energy. In fluoride glasses, its emission at 1.3 μm corresponds to the $^1G_4 \rightarrow {}^3F_4$ transition, which is suitable for optical amplification in the second telecommunication window [16].

The refractive indices in fluoroindate glasses doped with trivalent rare earth ions are typically around 1.49 ± 0.02. The thermal stability range of this family in glasses can vary depending on the concentration of their components. It is useful to study these parameters, as well as mechanical and spectroscopic characteristics, to optimize these materials for photonic applications. Also, it is useful to examine the effect of rare earth ions on these properties. In this work, we analyze the changes to the refractive index, thermal stability range and any potential laser transitions induced by substituting Ba for P in fluoroindate glasses doped with Nd^{3+} and Er^{3+} ions. We use absorption and luminescence spectroscopy and dif-

* Corresponding author. Tel.: +57 76 343495; fax: +57 76 343495.
E-mail address: aflorez@uis.edu.co (A. Flórez).

0925-8388/$ – see front matter. Published by Elsevier B.V.
doi:10.1016/j.jallcom.2009.09.046

ferential scanning calorimeter (DSC) measurements in samples of good optical quality. It is important to characterize the fluoroindate sample doped with Nd^{3+}, and as by adjusting the concentration of P in our samples, Ω_2 can change from a negative to a positive value.

2. Experimental analysis

2.1. Sample preparation

In this work, the goal is to analyze the effect of substituting BaF_2 for P_2O_5 in a fluoroindate glass (FI): $35InF_3$–$20ZnF_2$–$(16-x)BaF_2$–xP_2O_5–$20SrF_2$–$6GaF_3$–$2NaF$–REF_3; $x = 4.0$(FIP4); 8.0(FIP8); 12.0(FIP12), 16.0(FIP16); and RE = Er, Nd; 1.0 mol% concentration. The samples were prepared by using powders of oxides and fluorides of the highest available purity. Given the hygroscopic characteristics of fluorides and the strong instability of P_2O_5 in a moist environment, the samples were prepared in a chamber under a dry argon atmosphere. The transformation of the oxide into fluoride was accomplished by mixing the lanthanide, indium, gallium and phosphorus oxides with an excess (2× the stoichiometric amount) of ammonium bifluoride (NH_4FHF), and then heating the mixture in a platinum crucible at 400 °C for 3 h and 450 °C for 1 h for refining [17]. Then, the fluoride compounds were mixed and melted in a platinum crucible in a tubular furnace at 750 and 850 °C to refine and homogenise the liquid. The melt was then cast into a brass moult preheated to ≈260 °C and cooled at room temperature. The samples obtained showed good optical quality after cutting and polishing.

Density measurements were carried out using the Archimedes method in distilled water; the results varied between 5.02–4.76 and 4.98–4.67 g cm^{-3} ± 0.2 for Nd^{3+} and Er^{3+}, respectively. The refractive indices were measured using an Abbe refractometer; the contact liquid we used was 1-bromonaphthalin ($C_{10}H_7Br$). The results varied from 1.49 for FI to 1.56 for FIP16 doped with Nd^{3+} and 1.57 for FIP16 doped with Er^{3+}.

2.2. Absorption and luminescence spectra

Absorption spectra were recorded for all samples at room temperature on a double-beam UV–vis–NIR spectrophotometer (Jasco V-7200) in the spectral range of 300–3300 nm for the samples doped with Nd^{3+}, and a range of 300–2000 nm for samples doped with Er^{3+}. Given that the absorption path length changes from 0.16 to 0.31 cm in Nd^{3+} doped samples and from 0.13 to 0.24 cm in the Er^{3+} doped samples, the spectra for all samples, after subtracting the base line, were normalized in the optical density by their path length. Figs. 1 and 2 show the spectra for the three samples Er^{3+} and Nd^{3+} doped samples (FI, FIP4, and FIP8).

The oscillator strength was obtained from the area under the absorption band with the wavelength (λ) corresponding to the band baricenter using:

$$f = \frac{4.318 \times 10^{-9}}{Cl\lambda^2} \int K(\lambda) d\lambda \quad (1)$$

where K(k) is the spectral absorption coefficient, C[mol/l] is the concentration of the rare earth ion, and l[cm] is the path length.

The luminescence spectrum was obtained using a 150-W Xenon lamp and an appropriate filter. The emission from the sample was focused with an optical fiber on the entrance slit of a 490 ± 5 nm (DK480 of 0.5-m Spectral Products) monochromator. The emission was detected with a photomultiplier tube (Hamamatsu H5783-04) in the spectral range from 185 to 850 nm at room temperature, and recorded by a computerized data acquisition system. Fig. 3 shows the recorded spectrum for all the Er^{3+} doped samples.

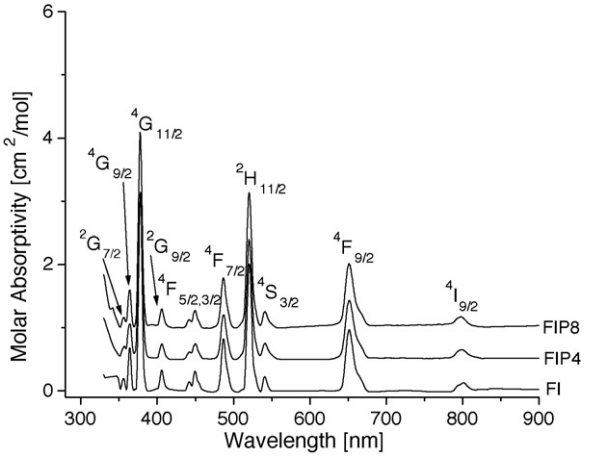

Fig. 1. Normalized absorption spectra at room temperature in the spectral range from 300 to 900 nm from ground state $^4I_{15/2}$ for all the samples doped with 1.0 mol% of Er^{3+} ions.

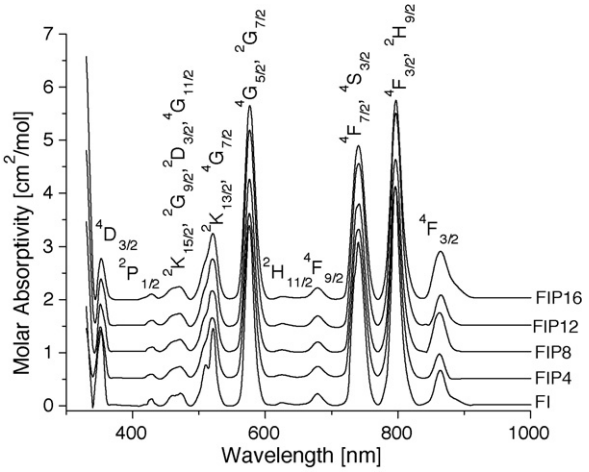

Fig. 2. Normalized absorption spectra at room temperature in the spectral range from 300 to 1000 nm from ground state $^4I_{9/2}$ for the all samples doped with 1.0 mol% of Nd^{3+} ions.

2.3. DSC measurements

The DSC measurements were recorded for the Nd^{3+} doped samples using a Differential Scanning Calorimeter (Q10 V8.1) from TA instruments at temperature range, from 30 to 600 °C, under an inert of atmosphere of N_2. The mass of the samples was 9.0 mg, and the heating rate was 10 °C min^{-1}. Fig. 3 shows the DSC curves for all samples.

3. Theoretical background

For trivalent lanthanide rare earth ions, the bands observed from absorption spectra correspond to intraconfigurational f-f transitions; the majority of these are induced electric dipole, and only a few of magnetic dipole transitions have been reported in these ions [15,18]. According to the Judd-Ofelt theory [13,14], the oscillator strength of a transition between two multiplets is given by:

$$f = \frac{8\pi^2 mc\sigma}{3h(2J+1)} \chi \sum_{\lambda=2,4,6} \Omega_\lambda \langle f^N \Psi' J' || U^{(\lambda)} || f^N \Psi J \rangle^2 \quad (2)$$

where m is the mass of the electron, c is the velocity of light, h is Planck's constant, σ is the mean energy (in cm^{-1}) for the tran-

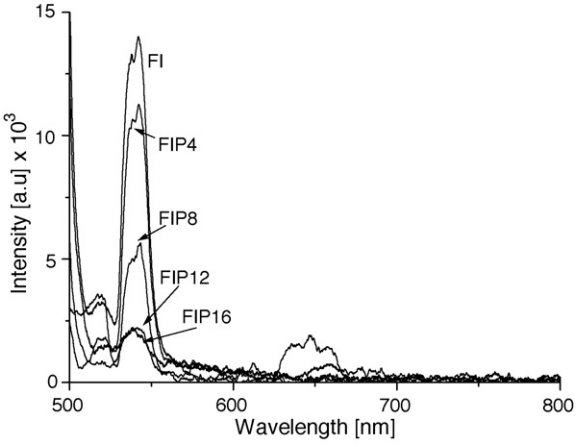

Fig. 3. Normalized luminescence spectra at room temperature in the spectral range from 500 to 800 nm for the all samples doped with 1.0 mol% of Er^{3+} ions. Excitation of the $^4F_{7/2}$ state is centered at 490 nm.

sition, and the factor $\chi = (n^2+2)^2/9n$ takes into account that the lanthanide ion is not in vacuum, but in a dielectric medium of refractive index n. $U^{(\lambda)}$ represents the squared reduced matrix elements $\langle f^N \psi' J' || U^{(\lambda)} || f^N \psi J \rangle^2$ of rank λ. Given that the matrix elements are virtually host independent, in this work we use the values reported by Carnall and co-workers for the trivalent lanthanide ions $Er^{3+}$and Nd^{3+} in LaF_3 [19].

The intensity parameters Ω_λ can be determined by a standard-least-square fitting method from the measured oscillator strengths by using Eq. (1). The quality of the fit is given by the magnitude of the root-mean-square ($\delta_{r.m.s.}$) deviation, as defined by:

$$\delta_{r.m.s.} = \left[\frac{\sum (f_{Cal} - f_{Exp.})^2}{(q-p)} \right]^{1/2} \quad (3)$$

where q is the equation number and p the parameter number.

Although the Judd–Ofelt model has been successful for the majority of lanthanide rare earths ions, there are ions for which the model does not work: Pr, Sm and Tb [20,21]. The model's fundamental assumptions about energy differences cause the most difficulty; in particular, the theory assumes that the difference in energy between $4f^N$ and $4f^N$–^{1}5d in all ions is large. Noting the energy differences (in cm^{-1}) in lanthanides: Pr (45,600), Nd (55,900), Sm (59,500), Eu (68,500), Tb (46,500), Dy (58,900), Ho (64,100), Er (64,200) and Tm (64,000) [22]; shows the inconsistency of the model, because Pr and Tb have similar values. This problem is reflected in the negative values taken by Ω_2 reported for Pr, Sm and Tb; these results are in contradiction with the definition of the Ω_λ parameters.

From the Judd–Ofelt intensity parameters Ω_λ, several radiative properties of the lanthanide ions can be calculated, such as the spontaneous emission coefficient, $A(\psi J, \psi' J') = A_{JJ'}$. This coefficient is given by the expression

$$A_{JJ'} = \frac{64\pi^4\sigma^3}{3h(2J+1)} \chi S_{ed} \quad \text{with}$$

$$S_{ed} = e^2 \sum_{\lambda=2,4,6} \Omega_\lambda \langle f^N \Psi J' \left\| U^\lambda \right\| f^N \Psi'' J \rangle^2 \quad (4)$$

where $\chi = n\,(n^2+2)^2/9$ is the effective field correction at a well-localized center in a medium of isotropic refractive index n, and S_{ed}, is the electric dipole line strength. Here, we do not take into account the magnetic dipole transitions. Once all emission probabilities that depopulate an initial level $^{2S+1}L_J$ have been calculated, they can be used to determine the rate at which that level is depopulated. This rate is given by the radiative lifetime $\tau_R(\psi J)$ defined as:

$$\tau_R(\Psi J) = \frac{1}{\sum_{\Psi' J'} A_{JJ'}} \quad (5)$$

4. Results and discussion

4.1. Absorption spectra

Figs. 1 and 2 show the normalized absorption spectra for samples doped with Er^{3+} and Nd^{3+}. The bands shown correspond to intraconfigurational f–f transitions that occur from the ground state $^4I_{15/2}$ for Er^{3+} and $^4I_{9/2}$ for Nd^{3+}. In the trivalent lanthanides, the free ion is only slightly perturbed by the crystal-field of the host. Each free-ion level, characterized by the total angular momentum J, is split by this field into a manifold of the more than $(2J+1)$ components. The splitting is usually not larger than 300 cm^{-1}. When we deal with ions in glasses, we neglect the site symmetry of the individual ions, such that the 41 electronic states that correspond to the configuration $4f^{11}$ of Er and the 41 states for the configuration $4f^3$ of Nd are reduced to 13 for Er and 19 for Nd. In order to label transitions that correspond to bands found from recorded absorption spectra, twelve bands for both ions in the ranges 300–1700 nm for Er^{3+} and 300–2600 nm for Nd^{3+}, we take the values reported by Carnall for these ions [23]. In the range shown in Figs. 1 and 2, the effect of the crystal field is larger in Er^{3+} than in Nd^{3+}. In that range, in Er^{3+} there is an overlapping of two components ($^4F_{5/2,\,3/2}$), whereas in Nd^{3+} for the same range there are five overlapping bands, four of which having two components: $^4F_{5/2}{}^*$ and $^2H_{9/2}$; $^4F_{7/2}$ and $^4S_{3/2}{}^*$; $^2K_{13/2}$ and $^4G_{7/2}{}^*$; the hypersensitive transition, $^4G_{5/2}{}^*$ and $^2G_{7/2}$; and the four single components $^2K_{15/2}$, $^2G_{9/2}{}^*$, $^2D_{3/2}$ and $^4G_{11/2}$. The overlap corresponding to the $^4G_{5/2}{}^*$ (hypersensitive) and $^2G_{7/2}$ bands centered at 571 and 573 nm, respectively, is very difficult to resolve even in crystal hosts. The effect on the absorption spectra by exchanging BaF_2 with P_2O_5 is not significant. Given this, the nominal concentration of doping was the same (1.0 mol%) for all glasses. The hypersensitive transitions in Er^{3+} ($^4I_{15/2} \rightarrow {}^2H_{11/2}$; $^4I_{11/2} \rightarrow {}^4G_{11/2}$) and Nd^{3+} ($^4I_{9/2} \rightarrow {}^4F_{5/2}{}^*$, $^2H_{9/2}$) are clearly identified by their strong intensity, and these transitions indicate that in these hosts the Er^{3+} and Nd^{3+} ions are not located at symmetric centers [15].

4.2. Oscillator strength and intensity parameters

A complicated problem with rare earth spectroscopy is the measurement and interpretation of the intensities of absorption bands. This problem is even more prevalent when ion hosts are glass materials. Given that the bands in glasses do not have a Gaussian shape, they exhibit inhomogeneous broadening associated with a variation of the crystal field from site to site, and the intensities must be measured using the area of the absorption bands. The intensity of spectral lines is measured using the oscillator strength given by Eq. (1). According to the Judd–Ofelt theory, the oscillator strength is a function of three phenomenological parameters Ω_λ, with $\lambda = 2, 4, 6$, and can be represented as a linear combination of these parameters. These parameters were determined by the method of least-square fitting using Eq. (2). The parameters are a function of the even and odd crystal field parameters, intraconfigurational radial integral and energy separation of the $4f^N$ states, and the opposite parity configurations. Hence, Ω_λ are dependent on the oscillator strength and are found to vary from site to site. In order to evaluate the validity of the intensity parameters Ω_λ obtained by the fitting, we calculate the root-mean-square values, $\delta_{r.m.s.}$, using Eq. (3). Tables 1–3 include the results of these calculations for all samples. From Table 1, the best fits are obtained in the Er^{3+} doped samples FIP12 and FIP16, (0.21).

From Table 1, the biggest difference between calculated and experimental oscillator strengths for all Er^{3+} doped samples was obtained in the transition corresponding to $^4I_{15/2} \rightarrow {}^4I_{13/2}$ centered at 1519 nm; this difference is not shown in Fig. 1, but decreases with an increasing concentration of P from 0.84 in FI to 0.39 in FIP16. Similarly, the deviation Δ of the hypersensitive transitions varied from 0.14 and 0.25 for FI to 0.10 and 0.16 for FIP16. These changes appear to be associated with the increasing number of F-P bonds around of the Er^{3+} ions [5].

An important aspect of Table 2 is that the $^4I_{9/2} \rightarrow {}^4D_{3/2}$ transition is not included in the calculation of the oscillator strength, because with it, $\Omega_2 < 0$ in the FI sample, as is shown in Table 3. Although, until now, there has not been a report of negative values for Ω_2 in Nd^{3+} in any host, this phenomenon can be understood given the ions' proximity to Pr^{3+} in the lanthanide series. Also, the problem has been associated with the small energy difference between the $4f^N$ and $4f^N$–^{1}5d configurations relative to the other ions in which Judd–Ofelt theory is successful [15]. Now, to avoid negative values for the Ω_2 parameter, various authors [16,24–26] often omit

Table 1
Calculated and experimental oscillator strength, ($f_{Cal.}$, f_{Exp}) × 10^{-6}, deviation, ($f_{Cal.}$–$f_{Exp.}$ = Δ) × 10^{-6} and root-mean-square deviation $\delta_{r.m.s.}$ × 10^{-6}, for all samples doped with Er^{3+}.

σ (nm)	FI			FIP4			FIP8			FIP12			FIP16		
	$f_{Cal.}$	$f_{Exp.}$	Δ	$f_{Cal.}$	$f_{Exp.}$	Δ	$f_{Cal.}$	$f_{Exp.}$	Δ	$f_{Cal.}$	$f_{Exp.}$	Δ	$f_{Cal.}$	$f_{Exp.}$	Δ
356	0.28	0.19	0.09	0.28	0.03	0.25	0.26	0.08	0.18	0.24	0.06	0.18	0.24	0.03	0.21
364	0.74	0.63	0.11	0.66	0.41	0.25	0.71	0.48	0.23	0.71	0.51	0.20	0.81	0.53	0.28
378*	3.36	3.50	0.14	3.29	3.36	0.07	3.62	3.68	0.06	3.75	3.83	0.08	4.36	4.46	0.10
406	0.47	0.30	0.17	0.47	0.26	0.21	0.43	0.28	0.15	0.39	0.31	0.08	0.40	0.37	0.03
449	0.63	0.39	0.24	0.65	0.36	0.29	0.57	0.47	0.10	0.52	0.43	0.09	0.52	0.43	0.09
487	1.14	0.86	0.28	1.13	0.82	0.31	1.05	0.93	0.12	0.99	0.84	0.15	1.04	0.93	0.11
521*	1.90	1.65	0.25	1.86	1.74	0.12	2.04	1.95	0.09	2.11	1.96	0.15	2.46	2.30	0.16
542	0.33	0.21	0.12	0.34	0.18	0.16	0.30	0.19	0.11	0.27	0.17	0.10	0.27	0.15	0.12
653	0.85	0.98	0.13	0.75	0.98	0.23	0.80	1.01	0.21	0.80	1.00	0.20	0.91	1.16	0.25
798	0.08	0.10	0.02	0.05	0.10	0.05	0.08	0.09	0.01	0.09	0.08	0.01	0.12	0.10	0.02
974	0.36	0.14	0.22	0.37	0.26	0.11	0.33	0.23	0.10	0.31	0.25	0.06	0.31	0.21	0.10
1519	0.80	1.64	0.84	0.82	1.70	0.88	0.74	1.22	0.48	0.68	1.12	0.44	0.69	1.08	0.39
$\delta_{r.m.s.}$	0.34			0.37			0.22			0.21			0.21		

* Hypersensitive transitions.

Table 2
Calculated and experimental oscillator strength, ($f_{Cal.}$, f_{Exp}) × 10^{-6}, deviation, ($f_{Cal.}$ − $f_{Exp.}$ = Δ) × 10^{-6} and root-mean-square deviation $\delta_{r.m.s.}$ × 10^{-6}, for all samples doped with Nd^{3+}.

σ (nm)	FI			FIP4			FIP8			FIP12			FIP16		
	$f_{Cal.}$	$f_{Exp.}$	Δ	$f_{Cal.}$	$f_{Exp.}$	Δ	$f_{Cal.}$	$f_{Exp.}$	Δ	$f_{Cal.}$	$f_{Exp.}$	Δ	$f_{Cal.}$	$f_{Exp.}$	Δ
353	–	3.23		2.36	2.79	0.43	1.43	1.06	0.37	2.27	2.23	0.04	1.80	1.32	0.48
426.5	0.32	0.23	0.09	0.34	0.16	0.18	0.19	0.11	0.08	0.32	0.17	0.15	0.25	0.30	0.05
466	0.66	0.77	0.11	0.73	0.58	0.15	0.53	0.58	0.05	0.69	0.80	0.11	0.60	0.74	0.14
518	2.62	3.06	0.44	2.66	2.84	0.18	2.15	2.82	0.67	2.82	3.40	0.58	2.50	3.14	0.64
576.5♦	5.30	5.27	0.03	5.51	5.50	0.01	5.65	5.60	0.05	6.70	6.66	0.04	6.61	6.56	0.05
628	0.08	0.05	0.03	0.08	0.04	0.04	0.07	0.03	0.04	0.09	0.07	0.02	0.08	0.05	0.03
679	0.29	0.28	0.01	0.29	0.28	0.01	0.28	0.25	0.03	0.32	0.29	0.03	0.30	0.29	0.01
740.5	3.76	3.68	0.08	3.62	3.53	0.09	3.75	3.50	0.25	4.16	4.02	0.14	3.99	3.72	0.27
797.5	3.70	3.73	0.03	3.65	3.54	0.11	3.31	3.48	0.17	3.99	4.15	0.16	3.65	3.75	0.10
865.5	1.24	0.66	0.58	1.28	0.38	0.90	0.85	0.66	0.19	1.26	0.49	0.77	1.03	1.09	0.06
1711.5	0.10	0.01	0.09	0.10	0.01	0.09	0.10	0.01	0.09	0.11	0.01	0.10	0.11	0.01	0.10
2458	0.76	0.68	0.08	0.73	1.61	0.88	0.76	0.74	0.02	0.84	0.54	0.30	0.81	1.06	0.25
$\delta_{r.m.s.}$	0.27; 0.34*; 0.34**			0.46			0.28			0.35			0.30		

0.27, 0.34*, and 0.34** correspond to the exclusion of the $^4I_{9/2} \rightarrow {}^4D_{3/2}$; $^4I_{9/2} \rightarrow {}^4G_{5/2}{}^*$, $^2G_{7/2}$ and $^4I_{9/2} \rightarrow {}^2K_{13/2}$,$^4G_{7/2}{}^*$ transitions, respectively; (♦) denotes a hypersensitive transition.

in the least-squares fitting in the Judd–Ofelt treatment of the $^3P_2$ state of Pr^{3+}, which corresponds to one transition. In this work, from the identified transitions, we omit several transitions, one at a time, and for Nd^{3+} doped samples, the results are shown in Table 4. Table 4 shows that there are several bands that give positive values of Ω_2 when different transitions are omitted; the exclusion of the hypersensitive transition, as suggested by most authors, is only one option. Additionally, in all cases treated in this work, the quality of fit as measured by the deviation $\delta_{r.m.s.}$ was similar for both bands calculated for all transitions and when calculated with some transitions omitted. Also, from Table 2, it is important to note that the fit corresponding to the hypersensitive transition is very good, and for all samples the deviation Δ changes from 0.01 to 0.05. The best fit ($\delta_{r.m.s}$ = 0.27) was obtained when we omitted the $^4I_{9/2} \rightarrow {}^4D_{3/2}$ transition in the FI sample; this values is similar to that of the FIP8 sample ($\delta_{r.m.s}$ = 0.28).

Table 3 gives the intensity parameters $\Omega_{2,4,6}$ for all samples doped with Er^{3+} and Nd^{3+}. For the Er^{3+} doped samples it is important to note that the values of Ω_2 in all of glasses are larger than $\Omega_{4,6}$. This behavior is not normal according to reports in the literature, as shown in the left part of Table 3. The values of which $\Omega_2 < 2.0$, in Er^{3+} and in Nd^{3+}, show strong covalent bonding, reflecting a high symmetry around the ions in all of the samples [15]. For Nd^{3+}, the right part of Table 3 shows that $\Omega_2 < \Omega_{4,6}$, which are the values normally observed for these parameters; also, the table shows that $\Omega_4 < \Omega_6$, as expected.

Table 4 shows the effect of progressively excluding the following transitions one at a time for a least-square fitting of the conventional Judd–Ofelt calculations: $^4I_{9/2} \rightarrow {}^4I_{11/2}$; $^4I_{9/2} \rightarrow {}^4F_{5/2}{}^*$, $^2H_{9/2}$; $^4I_{9/2} \rightarrow {}^4F_{7/2}$, $^4S_{3/2}{}^*$; $^4I_{9/2} \rightarrow ({}^4G_{5/2}{}^*, {}^2G_{7/2})^*$; and $^4I_{9/2} \rightarrow {}^4D_{3/2}$; $^4I_{9/2} \rightarrow {}^2K_{13/2}$,$^4G_{7/2}{}^*$. It is observed that the $\Omega_{2,4,6}$ parameters take exactly the same values with or without the $^4I_{9/2} \rightarrow {}^4I_{11/2}$ or $^4I_{9/2} \rightarrow {}^4F_{5/2}{}^*$, $^2H_{9/2}$ transitions. Also, it is clear that besides the hypersensitive transition there are other transitions which help in avoiding the negative values of Ω_2.

Table 3
Intensity parameters Ω_λ for all samples doped with Er^{3+} and Nd^{3+}, including all transitions identified from absorption spectra.

$\Omega_\lambda \times 10^{-20}$ cm^2	Er^{3+}					Nd^{3+}				
	FI	FIP4	FIP8	FIP12	FIP16	FI	FIP4	FIP8	FIP12	FIP16
Ω_2	1.2048	1.2545	1.3002	1.2905	1.4673	−0.0360	0.4171	1.1554	0.9222	1.2299
Ω_4	0.3755	0.2098	0.3761	0.4181	0.5556	3.3238	2.7038	1.5148	2.4404	1.8851
Ω_6	0.8997	0.9172	0.8013	0.7106	0.7044	2.5647	2.6157	2.7524	2.9074	2.8186

Table 4
Intensity parameters for the all Nd^{3+} doped samples, and transitions identified from absorption spectra that were excluded of the calculations of Ω_λ.

Transitions excluded of the calculates	$\Omega_\lambda \times 10^{-20}$ cm^2	FI	FIP4	FIP8	FIP12	FIP16
$^4I_{9/2} \rightarrow {}^4I_{11/2}$	Ω_2	−0.0574	0.3963	1.1854	0.9493	1.2465
	Ω_4	3.3520	2.7311	1.4752	2.4047	1.8631
	Ω_6	2.6161	2.6657	2.6802	2.8422	2.7786
$^4I_{9/2} \rightarrow {}^4F_{5/2}{}^*$, $^2H_{9/2}$	Ω_2	−0.0574	0.3963	1.1854	0.9493	1.2465
	Ω_4	3.3520	2.7311	1.4752	2.4047	1.8631
	Ω_6	2.6161	2.6657	2.6802	2.8422	2.7786
$^4I_{9/2} \rightarrow {}^4F_{7/2}, {}^4S_{3/2}{}^*$	Ω_2	−0.0734	0.4557	1.2562	0.9784	1.3354
	Ω_4	3.4046	2.6204	1.2968	2.3190	1.6569
	Ω_6	2.4034	2.7819	3.1872	3.1497	3.2738
$^4I_{9/2} \rightarrow ({}^4G_{5/2}{}^*$, $^2G_{7/2})^*$	Ω_2	0.9280	1.5917	5.9601	4.9646	5.6948
	Ω_4	3.2555	2.6205	1.1744	2.1540	1.5687
	Ω_6	2.5563	2.6054	2.7104	2.8721	2.7796
$^4I_{9/2} \rightarrow {}^4D_{3/2}$	Ω_2	0.4056	0.8951	0.7402	0.5237	0.8504
	Ω_4	2.5944	1.9144	2.2004	3.0995	2.4859
	Ω_6	2.7505	2.8167	2.5777	2.7315	2.8559
$^4I_{9/2} \rightarrow {}^2K_{13/2}, {}^4G_{7/2}{}^*$	Ω_2	0.0011	0.4628	1.3244	1.0637	1.3882
	Ω_4	3.2559	2.6203	1.2062	2.1820	1.5960
	Ω_6	2.5622	2.6126	2.7263	2.8979	2.8079

(·)* Hypersensitive transition.

Table 5 shows for all Er^{3+} doped samples the values of the spectroscopic parameters for the $^4F_{7/2}$ state and its low-lying relaxation states up to the ground state $^4I_{15/2}$, obtained from absorption spectra intensity parameters $\Omega_{2,4,6}$ and Eqs. (4) and (5). The table gives the values of all probabilities for only the FI sample. For the other samples, we include only the most significant probability values. From these values we note only a small effect of exchanging Ba for P. For FI and FIP4 samples, there is practically no change in $A_{JJ'}$ and τ_R.

4.3. Luminescence of the $^4F_{7/2}$ state excitation

Fig. 3 shows the luminescence spectra of Er^{3+} doped samples excited in the $^4F_{7/2}$ state centered in around 490 nm. Given that the spectra is normalized by the path length, and that the concentration of doping is the same in all samples (1.0 mol%), we note that the effect of exchanging BaF_2 for P_2O_5 in the $^4S_{3/2}$ transition is largest for the FI sample, smaller for the FIP4 sample, and smallest for the FIP8 sample; we also note quenching in the intensity luminescence in the FIP12 and FIP16 samples. Even for FIP8 the luminescence has an important value. Also, for FIP4 the transition from $^4F_{9/2}$ gives a nontrivial luminescence.

Table 5
Transitions, energy, σ, transition probability, $A_{JJ'}$ and radiative lifetime τ_R for all Er^{3+} doped samples.

Simple doped Er^{3+}	Transition	σ (cm^{-1})	$A_{JJ'}$	τ_R (ms)
FI	$^4F_{7/2} \rightarrow {}^2H_{11/2}$	1340	0.40	0.46
	$^4F_{7/2} \rightarrow {}^4S_{4/2}$	2084	1.49	
	$^4F_{7/2} \rightarrow {}^4F_{9/2}$	5220	23.49	
	$^4F_{7/2} \rightarrow {}^4I_{9/2}$	8003	84.65	
	$^4F_{7/2} \rightarrow {}^4I_{11/2}$	10267	178.74	
	$^4F_{7/2} \rightarrow {}^4I_{13/2}$	13951	448.44	
	$^4F_{7/2} \rightarrow {}^4I_{15/2}$	20534	1429.95	
FIP4	$^4F_{7/2} \rightarrow {}^4I_{9/2}$	8003	84.56	0.46
	$^4F_{7/2} \rightarrow {}^4I_{11/2}$	10267	178.56	
	$^4F_{7/2} \rightarrow {}^4I_{13/2}$	13951	447.97	
	$^4F_{7/2} \rightarrow {}^4I_{15/2}$	20534	1428.46	
FIP8	$^4F_{7/2} \rightarrow {}^4I_{9/2}$	8003	81.13	0.48
	$^4F_{7/2} \rightarrow {}^4I_{11/2}$	10267	171.31	
	$^4F_{7/2} \rightarrow {}^4I_{13/2}$	13951	429.78	
	$^4F_{7/2} \rightarrow {}^4I_{15/2}$	20534	1370.04	
FIP12	$^4F_{7/2} \rightarrow {}^4I_{9/2}$	8003	78.03	0.50
	$^4F_{7/2} \rightarrow {}^4I_{11/2}$	10267	164.76	
	$^4F_{7/2} \rightarrow {}^4I_{13/2}$	13951	413.17	
	$^4F_{7/2} \rightarrow {}^4I_{15/2}$	20534	1318.11	
FIP16	$^4F_{7/2} \rightarrow {}^4I_{9/2}$	8003	84.37	0.46
	$^4F_{7/2} \rightarrow {}^4I_{11/2}$	10267	178.15	
	$^4F_{7/2} \rightarrow {}^4I_{13/2}$	13951	446.96	
	$^4F_{7/2} \rightarrow {}^4I_{15/2}$	20534	1425.22	

4.4. DSC measurements

Fig. 4 shows the differential scanning calorimeter graphs for the Nd^{3+}doped glasses. We have assumed that only minimal changes might appear in the results analyzing the graphs for only one ion. From the graphs we obtained T_g, T_x and ΔT. It is observed that in the temperature range scanned, there is little tendency to form crystalline phases in the FIP16 sample. The stability range obtained for the samples was: 121.7 °C (FI); 155.37 °C (FIP4); 167 °C (FIP8); 114.11 °C (FIP12) and 177.17 °C (FIP16) all with ±5.0 °C. From the results we observe that the sample with the largest content of P (FIP16) presents the largest stability range. Only the analysis of FIP4 can take into account the results of the previous samples; we find that155.37 ± 5.0 °C, (T_g = 310.36 °C and T_x = 465.73 °C).

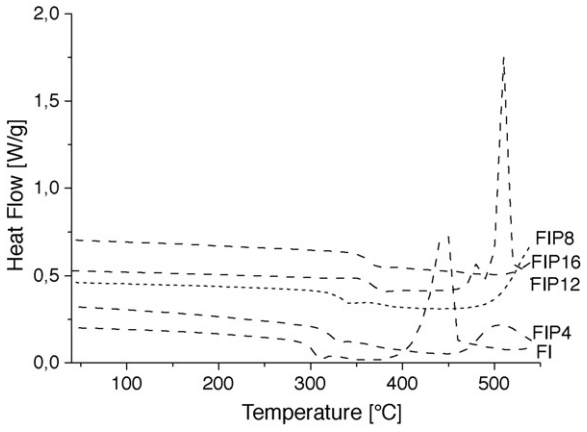

Fig. 4. DSC measurements in the temperature range from 30 to 600 °C for all of the samples doped with 1.0 mol% of Nd^{3+}.

5. Conclusions

This study shows that fluoroindate glasses modified and optimized with lanthanide ions have potential for laser applications. Concentrations larger than 8.0 mol% have a strong tendency to produce quenching in the fluoroindate glasses. The presence of P in the fluoride glasses can contribute to increasing the thermal stability. In that sense, of the glasses analyzed in this work, the sample with 4.0 mol% of P_2O_5 showed the best properties. The Ω_2 of Nd^{3+} ion in fluoroindate glasses shows the tendency towards negative Ω_2 values. Since the values are normally take $\Omega_2 \leq 2$ in these glasses, we conclude that there is high symmetry and covalence around the rare earth ions. Finally, in the Er^{3+} doped samples is noted that, $\Omega_2 > \Omega_{4,6}$, which is unusual in these host materials.

Acknowledgements

This work was partially supported by The Excellence Center for Novel Materials – ECNM, under Contract No. 043-2005 subscribed with Colciencias; and the Foundation for the Promotion of Research and Technology of the Bank of the Republic.

References

[1] Marcel Poulain, J. Non-Cryst. Solids 184 (1995) 103–108.
[2] F. Auzel, J. Alloys Compd. 275–277 (1998) 692–696.
[3] M. Mortier, P. Goldner, P. Féron, G.M. Stephan, H. Xu, Z. Cai, J. Non-Cryst. Solids 326 and 327 (2003) 505–509.
[4] Jean-Luc Adam, J. Fluorine Chem. 107 (2001) 265–270.
[5] Joanna Pisarska, Bozena Kaczmarczyk, Zbigniew Mazurak, Micha Zelechower, Tomasz Goryczka, Wojciech A. Pisarski, Physica B 388 (2007) 331–336.
[6] Fluoride Glass for Optical Fibers, P.W. France–Blackie, London, 1990.
[7] J. Schneider, C. Carbonnier, U.B. Unrau, Appl. Opt. 36 (1997) 8595.
[8] R. Reisfeld, C.K. Jorgensen, Excited State Phenomena in Vitreous Materials, Handbook on the Physics and Chemistry of Rare Earths, Elsevier Science Publishers, 1987 (Chapte.58).
[9] J.H. Campbell, T.I. Suratwala, J. Non-Cryst. Solids 263&264 (2000) 318–341.
[10] J.H. Campbell, 25 years of laser glass development leading to a 1.8 MJ, 500 TW laser for fusion ignition, Lawrence Livermore National Laboratory Report, UCRL-JC-129507, 1998, p. 1.
[11] C.K. Jayasankar, R. Balakrishnaiah, V. Venkatramu, A.S. Joshi, A. Speghini b, M. Bettinelli, J. Alloys Compd. 451 (2008) 697–701.
[12] J. Pisarska, W. Ryba-Romanowski, G. Dominiak-Dzik, T. Goryczka, W.A. Pisarski, J. Alloys Compd. 451 (2008) 223–225.
[13] B.R. Judd, Phys. Rev. B 127 (1962) 750.
[14] G.S. Ofelt, J. Chem. Phys. 37 (1962) 511.
[15] R.D. Peacok, Struct. Bond. 22 (1975) 83.
[16] R.S. Quimby, W.J. Miniscalco, J. Appl. Phys. 75 (1) (1994) 613–615.
[17] M. Poulain, G. Mazé, Chemtronics 3 (1998) 77.
[18] C. Görller-Walrand, K. Binnemans, Spectral intensities of f–f transitions, in: K.A. Gschneidner Jr., L. Eyring (Eds.), Handbook on the Physics and Chemistry of Rare Earths, vol. 25, 1998, p. 101 (ch. 167, North-Holland, Amsterdam).
[19] W.T. Carnall, P.R. Fields, K. Rajnak, J. Chem. Phys. 49 (10) (1968) 4424–4442.
[20] A. Flórez, A. Herrera, M. Flórez, Phys. Stat. Sol. (c) 4 (11) (2007) 4156–4164.
[21] A. Florez, M. Brik, O. Plata, J. Mater. Sci.: Mater. Electron. 20 (2009) S230–S234.
[22] R. Reisfeld, C.K. Jorgensen, Laser and Excited States of Rare Earth, Springer Verlag, Berlin, 1977.
[23] W.T. Carnall, H. Crosswhite, H.M. Crosswhite, Energy level structure and transitions probabilities of the trivalent lanthanides in LaF_3, Argonne National Laboratory, Special Report, 1977.
[24] M. Eyal, E. Greemberg, R. Reisfield, N. Spector, Chem. Phys. Lett. 117 (2) (1985) 108.
[25] W. Seeber, E.A. Downing, L. Hesselink, M.M. Fejer, D. Ehrt, J. Non-Cryst. Solids 189 (1995) 218–226.
[26] H. Inoue, K. Soga, A. Makishima, J. Non-Cryst. Solids 325 (2003) 282–294.